Soler, M., González-Arribas, D., Sanjurjo-Rivo, M., García-Heras, J., Sacher, D., Gelhardt, U., Lang, J., Hauf, T., & Simarro, J. (2020). Influence of atmospheric uncertainty, convective indicators, and cost-index on the leveled aircraft trajectory optimization problem. *In Transportation Research Part C: Emerging Technologies, 120*, 102784-102803.

DOI: 10.1016/j.trc.2020.102784

Influence of atmospheric uncertainty, convective indicators, and cost-index on the leveled aircraft trajectory optimization problem

Manuel Soler[a], Daniel González-Arribas[a], Manuel Sanjurjo-Rivo[a], Javier García-Heras[a], Daniel Sacher[b], Ulrike Gelhardt[b], Jürgen Lang[b], Thomas Hauf[c], Juan Simarro[d]

[a] *Department of Bioengineering and Aerospace Engineering, Universidad Carlos III de Madrid. Avenida de la Universidad, 30, Leganés (28911 Madrid), Spain. e-mail: masolera@ing.uc3m.es (corresponding author), daniel.gonzalez.arribas@ing.uc3m.es, msanjurj@ing.uc3m.es, gcarrete@ing.uc3m.es*

[b] *MeteoSolutions GmbH. Wilhelminenstrasse 2, D-64283, Darmstadt (Germany)*

[c] *Leibniz University of Hannover. e-mail: hauf@muk.uni-hannover.de*

[d] *Agencia Estatal de Meteorología (AEMET), Valencia, Spain. e-mail: jsimarrog@aemet.es*

Abstract

The existence of significant uncertainties in the models and systems required for trajectory prediction represents a major challenge for the Air traffic Management (ATM) system. Weather can be considered as one of the most relevant sources of uncertainty. Understanding and managing the impact of these uncertainties is necessary to increase the predictability of the ATM system. State-of-the-art probabilistic forecasts from Ensemble Prediction Systems are employed to characterize uncertainty in the wind and potential convective areas. A robust optimal control methodology to produce efficient and predictable aircraft trajectories in the presence of these uncertainties is presented. Aircraft motion is assumed to be at a constant altitude and variable speed, considering BADA4 as the aircraft performance model. A set of Pareto-optimal trajectories is obtained for different preferences among predictability, convective risk, and average cost index running a thorough parametric study on a North Atlantic crossing use case. Results show that the cost of reducing the arrival time window by 10 sec. is between 100 to 200 kg or 3 to 6 min., depending on the cost-index. They also show that reducing the exposure to convection by 50 km is on the order of 5 to 10 min. or 100 to 200 kg. of average fuel consumption.

Preprint submitted to Transportation Research Part C: Accepted version.Vol. 120, 2020, https://doi.org/10.1016/j.trc.2020.102784 Ja

Keywords: optimal control, robust planning, convective weather, aircraft trajectory planning

1. Introduction

The Air Traffic Management (ATM) system in the busiest airspaces in the world is currently being overhauled to deal with multiple capacity, socioeconomic, and environmental challenges. One major pillar of this process is the shift towards a concept of operations centered on aircraft trajectories instead of rigid airspace structures. However, its successful implementation rests on appropriate understanding and management of uncertainty.

Due to its complex socio-technical structure, the operation of the ATM system is heavily impacted by uncertainty, emerging from multiple sources and propagating through the interconnections between its subsystems. Any analysis of uncertainty in the ATM system should take into account different scales with their respective sources. Refer to [**?** , Chapter 4] for a thorough description of uncertainties impacting the ATM system, with weather recognised as one of its major contributors. Due to its nonlinear and chaotic nature, some meteorological phenomena, especially those related to convection, cannot be forecasted with complete accuracy at any arbitrary lead time with the required accuracy. This then leads to a general uncertainty or disruption for individual air and ground operations, which then propagates through all ATM processes. It is, therefore, necessary to deal with meteorological uncertainty at multiple scales, and its impact on the trajectory prediction and planning processes and trajectory execution. The focus of the present paper is on flight uncertainty and pre-departure temporal scale (flight dispatching planning level, from two/three hours up to off-block time).

Ensemble Prediction Systems (EPS) provide probabilistic meteorological forecasts. They seek to provide an estimation of the uncertainty that is inherent to the Numerical Weather Prediction (NWP) process [**?**], and thus to overcome the limitation of a single deterministic forecast. In an EPS, several

runs of the NWP model are launched with slightly different characteristics to produce a set of (typically) 10 to 50 different forecasts or "members" of the ensemble. We refer to [**?**] for a review of the status of NWP as well as the relevance of EPS in a wider meteorological context.

Recent attention has been put into analyzing meteorological hazards and their effects on flight planning. For instance, Kin et al. have considered combined effects of both winds and clear air turbulence (note that clear air turbulence is not considered in this paper) [**?** **?**]. Other works have recently focused on winds and its associated uncertainty. For instance, in [**?**], González-Arribas et al. studied the flight planning problem under wind uncertainty using robust optimal control. The same problem has been solved with two additional approaches: In [**?**] Franco et al. presented a hierarchical, bi-level flight planning algorithm in which they combined the Dijkstra algorithm (high-level) with a trajectory predictor (low-level) based on a probabilistic transformation; and Legrand et al. in [**?**], who solve the problem with an approach based on dynamic programming.

If we focus on convective phenomena, there is substantial ongoing work on short-term hazard avoidance close to the encounter, when the information on the location and short-term evolution of the storm cell is available though still with some uncertainty. Just to cite a few, in [**?** **?** **?**] the focus is on en-route problems, whereas in [**?** **?**] the focus is on terminal airspaces. Indeed, tools that incorporate different path planning algorithms for tactical convective weather avoidance are in use today, e g.. the so-term Dynamic Multi-Flight Common Route Advisories system [**?** **?**] or the Convective Avoidance Weather Model (CWAM) [**?**]. On the contrary, the consideration of convective risk in flight planning algorithms (at a larger time scale of 1 to 3 hours before departure) has not received enough attention so far.

This is based on the fact that for the time scales of 1-3 hours we only know the area within which individual convective storms may develop. This area of potentially developing storms is referred to as convective area. The onset and the location of individual storms within a convective area, however, is currently and

for the near future not possible to forecast at the given time scale. Nevertheless, some basic characteristics of those storms can be derived prior to any convective development, which are necessary but not sufficient conditions for the formation of storms (thermodynamic stability of the air mass). That information can be employed to create an index that estimates the probability of convection, i.e., an indicator of convection risk that can be used for trajectory planning. Convective areas may have a persistence up to 60 hours for tropical latitudes, travelling with their surrounding air mass. They shall not necessarily be avoided but require a higher weather situation awareness by pilots and controllers. Trajectories, however, leading through convective areas might experience significant changes due to suddenly developing storms, which results in increased flight duration and delays. The dimension of the latter depends, among other factors, on the type of storms embedded in the convective area, density of cells, their orientation, the size of gaps separating the storms and the time of onset.

Preliminary work on robust optimal control with application to flight planning in which we consider both uncertainties associated with winds and convective areas was presented in [**?**]. Both the altitude and the true airspeed were considered constant. The main contribution of the present paper is to extend this work to the consideration of variable speed profiles, BADA4 aircraft performance modelling (which, contrary to BADA 3, incorporates compressibility effects to model drag forces) and the introduction of cost-index based operational cost. We applied this methodology to a case study assuming the altitude to be constant.

The paper is structured as follows: we introduce convection and its associated indicators in Section 2. The robust optimal control methodology and its application to flight planning is presented in Section 3 and Section **??**. In Section 4, we present a case study, including the simulation results and a discussion. Finally, some conclusions are drawn in Section 5.

2. Convection Modelling

2.1. Ensemble Prediction Systems (EPS)

An EPS produces a collection of forecasts for the same prediction time that constitutes a representative sample of the possible future states of the atmosphere. An ensemble is typically composed of 10 to 50 individual forecasts referred to as members. To produce the different members, NWP centers employ combinations of several techniques, including changing initial conditions in the most sensitive directions, changing the parameters of the simulation, combining different models or building time-lagged ensembles. Those variations, however, are considered as physically equal. But the resulting ensemble members may differ notably from each other with those differences emerge from e.g. small differences in the initial conditions. Please refer to [**? ? ? ?**].

2.1.1. Characteristics

For deterministic medium-range prediction, the typical setup of a forecasting system is a dynamical core with a resolution of around 15 km (horizontal) and 80 levels. The dynamical core might be hydrostatic or as in more advanced models fully compressible. Standard practices involve running the model 2 or 4 times a day, with output at a 1-, 3-, or 6-hour intervals.

For deterministic short-range prediction, the model is restricted to a limited area, non-hydrostatic effects are taken into account, and the resolution is improved to a horizontal grid of 1.5 to 5 km. Runs are also shorter (around a day of output) and run more frequently (from 4 to 8 times a day).

Since ensemble predictions require multiple model runs (10 to 50) for the same time interval, lower resolutions compared with the deterministic systems are used. The horizontal resolution is typically around twice the resolution for the deterministic prediction, and the vertical levels are also reduced. Depending on the area of interest and the target time interval, ensemble predictions can be classified in three categories:

- Global, medium-range forecasts are run for the whole globe and usually aim at forecasting 2 to 10 days ahead. They capture the uncertainty associated with planetary-level perturbations.

- Limited Area Models (LAM), short-range forecasts predict weather in a specific region at a 1-2 day timescale. The associated uncertainty captured by LAM forecasts is associated with mesoscale-alpha phenomena (200-2000 km characteristic scales).

- LAM, very short range forecasts produce predictions for a time-horizon of a few hours. The uncertainty is related to mesoscale-beta (20-200 km) and mesoscale-gamma (2-20 km) phenomena.

2.1.2. Medium-range ensemble forecasting

The World Meteorological Organization launched the THORPEX (The Observing System Research and Predictability Experiment) research initiative in 2004 to stimulate the development, usage, utility and accuracy of medium-range ensemble forecasts. Importantly, it created the TIGGE dataset[1] [**?**].

TIGGE contains global medium-range ensemble forecast data produced by several NWP centers for scientific research [**?**] in a homogeneous format. It is hosted on the website of the European Center for Medium-Range Weather Forecasts (ECMWF).[2] The ECMWF [**?**], the Canadian Meteorological Center [**?**] and the National Center for Environmental Prediction (NCEP) [**?**], among others, develop ensemble prediction systems included in TIGGE. ECMWF EPS has nowadays a horizontal resolution of 18 km to be able to forecast the weather at the whole globe for 2 to 10 days. Nevertheless, as hardware becomes more efficient and less expensive, the NWP upgrade their systems to increase the resolution of their forecasts.

In 2014, the TIGGE-LAM dataset was also launched to include regional ensembles on finer (from 2 to 10 km) grids.

[1] http://tigge.ecmwf.int/documents/
[2] http://apps.ecmwf.int/datasets/

2.1.3. LAM *ensemble forecasting*

By limiting the area and period of interest, LAMs can use a higher resolution. Examples of these models include: The UK Met's MOGREPS [**?**]; the AEMET's SREPS [**?**] ensemble; the Norwegian Meteorological Institute's LAMEPS [**?**] the COnsortium for Small-scale MOdelling's COSMO-LEPS [**?**] Météo France's PEARP [**?**]. LAMs often focus on land regions to study the weather in areas of greater impact on human activities; as a consequence, their oceanic and maritime coverage is often limited.

2.2. Convection Indicators

We attempt to delimit high-risk areas due to deep convection (vertical range up to the top of the troposphere) and their respective uncertainty. "Convective area" is herein defined as an area of potentially developing storms, which comprise events such as individual storm cells, multi-cells, mesoscale convective complexes and squall lines. Favourable environmental characteristics and conditions for the development of some of these types of convective phenomena include e.g.:

- A squall line (at least in Central Europe) very often develops several hundred kilometers ahead of and parallel to an approaching cold front. It is accompanied and recognized prior to its development by a boundary convergence line. Many such lines are often separated approx. 10 km, but not all of them necessarily develop into a squall line, though some of them do.

- Air mass storms preferably develop in the afternoon. The onset time of first shallow clouds and the development of deep convective clouds can be forecasted by standard meteorological procedures.

- Moderate mid-level shear enhances the storm strength, while extremely strong shear and no-shear environments are more likely related to weak storms.

- Long-lived storms are linked to the renewal and generation of new cells immediately ahead of a mature cell.

- Storms embedded in a cold front, which are out of the scope of this study as they can be forecasted very well by synoptic forecasts of low pressure systems.
- The structure of the environmental temperature profile allows deriving certain features of the storm. Maritime dominated storms reveal a temperature profile close to the moist-adiabatic implying weak updrafts, while continental storms exhibit more potential energy to be released. The latter is defined by the area between the temperature profile and the moist adiabatic of a given air parcel if it rose from the surface vertically through the entire atmosphere.

Important to note is that the above characteristics are necessary conditions for convection, but they do not allow the forecast of the precise location, extension, onset, duration, intensity, and movement. Convective storms require a trigger mechanism that needed to be forecasted (if possible). Trigger mechanisms such as boundary convergence lines, tropospheric gravity waves, mountains or surface temperature inhomogeneities provide the needed lift to initiate convection.

From the above, we conclude that we need an indicator to describe the necessary precondition for the potential development of convection, which comprises the essential activator to develop a storm. This will be done by using a combination of two convection indicators, namely *Total Totals Index* and *Convective Precipitation*, which are both available as part of an EPS forecast.

2.2.1. Total Totals Index (TT)

[3] TT is the sum of the vertical totals (VT) and the cross totals (CT), where:

$$VT = T_{850} - T_{500}$$

is the temperature gradient between 850 hPa and 500 hPa, and

$$CT = T_{d_{850}} - T_{500}$$

[3] attributable to National Weather Service Louisville, KY: http://www.weather.gov/lmk/indices, accessed July 25, 2016.

	Thunderstorm activity			
TT_i	Moderate	Heavy	Severe	Tornadoes
< 44	-	-	-	-
44-45	Isolated	-	-	-
46-47	Scattered	Few	-	-
48-49	Scattered	Few	Isolated	-
50-51	*	Scattered	Few	Isolated
52-55	*	Numerous	Few/scattered	Few
> 55	*	Numerous	Scattered	Scattered

Table 1: Operational taxonomy of risk of severe weather activity.

is the moisture content between 850 hPa and 500 hPa by subtracting the temperature in 500 hPa from dew point temperature in 850 hPa.

As a result, TT accounts for both static stability and 850 hPa moisture but would be unrepresentative in situations where the low-level moisture resides below the 850 hPa level. Also, convection may be inhibited despite a high TT value if a significant capping inversion is present. $VT = 40$ is close to dry adiabatic for the 850-500 hPa layer. However, VT generally will be much less, with values around 26K or more, representing sufficient static instability (without regard to moisture) for thunderstorm occurrence. $CT > 18$K often is necessary for convection, but the combined TT is more correlated to convection than its components (VT and CT) separately. The risk of severe weather activity is operationally defined as in Table 1 (see also [**?**]).

2.2.2. Convective Precipitation (CPre)

[4] CPre is a model output quantity and is an estimation of the precipitation coming from convective clouds. The total model precipitation is the sum of the

[4]ECMWF, Reading, UK, accessed July 25, 2016:
http://www.ecmwf.int/en/research/modelling-and-prediction/atmospheric-physics.

so-called large-scale precipitation and the convective precipitation.

The moist convection scheme, we are here referring to, is based on the mass-flux approach and represents deep (including *cumulus congestus*), shallow and mid-level (elevated moist layers) convection. The distinction between deep and shallow convection is made based on the cloud depth ($<$ 200 hPa for shallow). For deep convection the mass-flux is determined by assuming that convection removes the so-called Convective Available Potential Energy (CAPE) over a given time scale. The intensity of shallow convection is based on the budget of the moist static energy, i.e. the convective flux at cloud base equals the contribution of all other physical processes when integrated over the sub-cloud layer. Finally, mid-level convection can occur for elevated moist layers, and its mass flux is set according to the large-scale vertical velocity. The scheme, originally described in Tiedtke [**?**], has evolved over time and amongst many changes includes a modified entrainment formulation leading to an improved representation of tropical variability of convection [**?**], and a modified CAPE closure leading to a significantly improved diurnal cycle of convection [**?**]. The mass flux scheme, in other words, imitates the net effect of convection and rearranges atmospheric layers towards a thermodynamic stable static atmosphere.

2.3. Calculation of probability of convention/clear air

Using the grid-based output of TT and CPre from the ECMWF-EPS data, which results in TT and CPre values for each member at the horizontal nodes of the desired sub-grid. With this information, we compute an ensemble-based probability of convection/clear air for each grid point.

Probability of convection: The ensemble-based probability of convection is the fraction of ensemble members with values above the given thresholds TT_H and $CPre_H$ for all TT and $CPre$ of the ensemble members. For TT_H we suggest one of the threshold values given in Table 1. For $CPre_H$ we suggest 0; which means that any given amount of convective precipitation originates from convective events:

$$p_c = \frac{N_c}{N}, \tag{1}$$

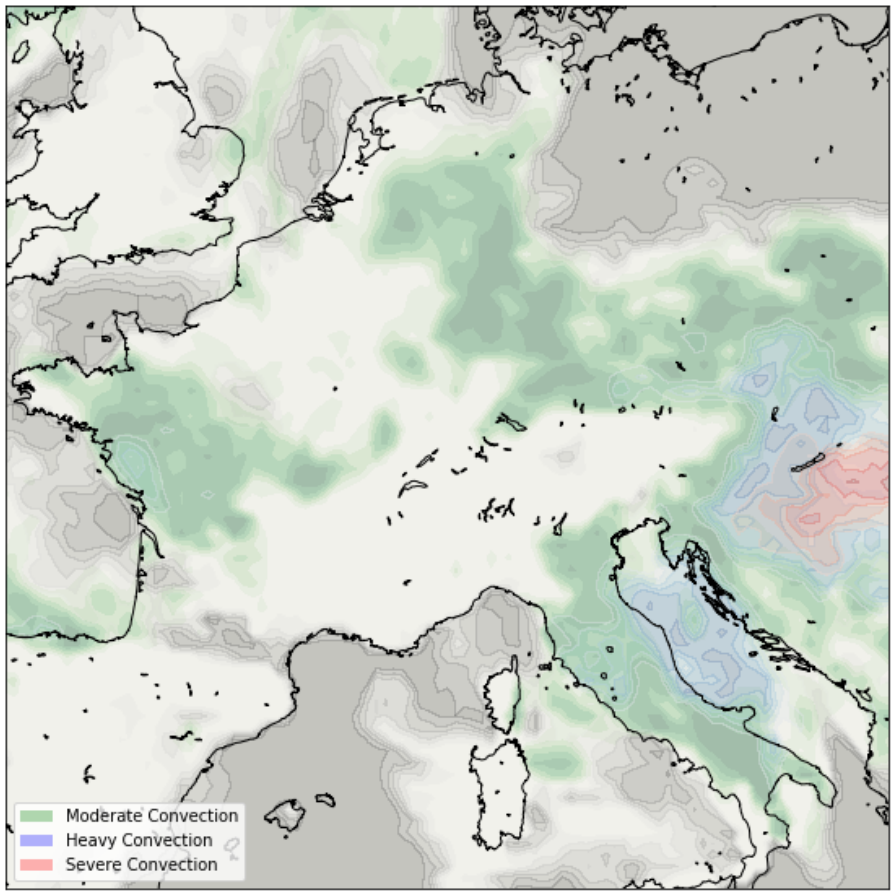

Figure 1: Schematic illustration of the suggested classification of convective activity. In the coloured ares, one can distinguish red (severe), blue (heavy), and green (moderate) convective activity.

where N is the numbers of ensemble members, $N_c = \sum_{i=1}^{N} i$, and so that $TT_i > TT_H \wedge CPre_i > CPre_H$. This probability of convection (p_c) will be used in Eq. 17 to compute the objective function.

Probability of clear air: This value shows regions of clear air with low uncertainty:

$$p_{nc} = \frac{N_{nc}}{N}, \tag{2}$$

where N is the numbers of ensemble members, $N_{nc} = \sum_{i=1}^{N} i$, and so that $TT_i \leq TT_H \wedge CPre_i \leq CPre_H$.

3. Robust Trajectory Planning Methodology

We consider the problem of flight planning, i.e., 1-3 hours before departure. To model uncertainties in the weather forecast, we rely on EPS forecasts. The uncertainty will be represented with a quadrature rule where each member of the EPS forecast corresponds to a quadrature point. Each scenario will be weighted equally; if the EPS contains N members, then the weight of each member is $w_k = 1/N$. The approach is based on a robust optimal control approach to aircraft trajectory optimization problems [**?**]. We will summarize the method and incorporate the convective indicator.

3.1. Robust Optimal Control

Let us consider a dynamical system given by a randomly parametrized differential-algebraic equation with constraints. Uncertainty is described using a standard Kolmogorov probability space $(\Omega, \mathscr{F}, P)$; it is composed by a sample space of possible outcomes Ω, a σ-algebra of events $\mathscr{F}$ containing sets of outcomes, and the probability function P that assigns a probability to each of these events. The uncertain parameters of the system will be modeled as a *constant* random variable $\xi : \Omega \to \mathbb{R}^{n_\xi}$. For each possible outcome $\omega \in \Omega$, the random variables take a different value $\xi(\omega)$.

Let us denote the state vector by $\mathbf{x} \in \mathbb{R}^{n_x}$, the control vector by $\mathbf{u} \in \mathbb{R}^{n_u}$, the algebraic variables by $\mathbf{z} \in \mathbb{R}^{n_z}$ and $t \in \mathbb{R}$ as independent variable (usually time). For each outcome $\omega_0 \in \Omega$, there exist a unique trajectory path $t \to (\mathbf{x}(\omega_0, t), \mathbf{z}(\omega_0, t), \mathbf{u}(\omega_0, t))$ that corresponds to the realization of the random variables $\xi(\omega_0)$. The dynamics of the system are given by the functions $f : \mathbb{R}^{n_x} \times \mathbb{R}^{n_z} \times \mathbb{R}^{n_u} \times \mathbb{R}^{n_\xi} \times \mathbb{R} \to \mathbb{R}^{n_x}$, $h : \mathbb{R}^{n_x} \times \mathbb{R}^{n_z} \times \mathbb{R}^{n_u} \times \mathbb{R}^{n_\xi} \times \mathbb{R} \to \mathbb{R}^{n_h}$, and $g : \mathbb{R}^{n_x} \times \mathbb{R}^{n_z} \times \mathbb{R}^{n_u} \times \mathbb{R}^{n_\xi} \times \mathbb{R} \to \mathbb{R}^{n_g}$, such that valid trajectories fulfill

the conditions almost surely (i.e. with probability 1):[5]

$$\frac{d}{dt}\mathbf{x}(\omega,t) = f(\mathbf{x}(\omega,t),\mathbf{z}(\omega,t),\mathbf{u}(\omega,t),\xi(\omega),t), \tag{3}$$

$$h(\mathbf{x}(\omega,t),\mathbf{z}(\omega,t),\mathbf{u}(\omega,t),\xi(\omega),t) = 0, \tag{4}$$

$$g_L \leq g(\mathbf{x}(\omega,t),\mathbf{z}(\omega,t),\mathbf{u}(\omega,t),\xi(\omega),t) \leq g_U, \tag{5}$$

where $\omega \in \Omega$ is the sample point on the underlying abstract probability space and g_L and g_U are lower and upper bounds. Therefore, for each possible scenario or realization of the random parameters $\xi(\omega)$, the trajectory will follow the deterministic differential equation (3) for the corresponding fixed value of ξ. We employ the notation $\mathbf{x}(\omega,t)$ and $\mathbf{u}(\omega,t)$ to emphasize the fact that the trajectory depends on the realization of the random parameters.

The optimal *guidance* scheme relies herein on the notion of *tracked* states:

Definition 3.1. A state is said to be *tracked* if its trajectory is assumed to be independent of the realization of the random variables almost surely, i.e. with probability of one.

In such optimal *guidance* scheme, some of the states are "tracked" (i.e. identical in all scenarios) and the controls are specific to each scenario to guarantee that the tracked states follow the unique computed trajectory. The associated practical concept demands that the controls can be computed online in this fashion to follow a guidance path; this condition is verified in aircraft trajectory planning, where the pilot or the autopilot can manage the aircraft to follow the route and the vertical profile.

Definition 3.2. The amount *control degrees of freedom* d of the dynamical system is defined herein as the number of controls and free algebraic variables minus the number of algebraic restrictions: $d = n_z + n_u - n_h$.

[5] The $\leq$ sign applies in an element-wise fashion in Equation (5) and analogous equations.

Let $q_x \leq \min\{n_x, d\}$ be the number of tracked states; without loss of generality, we can assume that the tracked states are the first q_x states (rearrange the state vector otherwise), i.e.

$$\mathbf{x} = \begin{bmatrix} x_1 & \dots & x_{q_x} & x_{q_x+1} & \dots & x_{n_x} \end{bmatrix}^T = \begin{bmatrix} \mathbf{x}_q \\ \mathbf{x}_r \end{bmatrix},$$

where $\mathbf{x}_q$ is the tracked part of the state vector and $\mathbf{x}_r$ is the untracked part. Let $\mathbb{I}_n$ be the identity matrix of shape $n \times n$ and $0_{n_1,n_2}$ be the zero matrix (i.e. a matrix with zeroes in all its entries) of shape $n_1 \times n_2$. We define the matrix $E_x \in \mathbb{R}^{q_x \times n_x}$ as

$$E_x = \begin{bmatrix} \mathbb{I}_{q_x} & 0_{q_x, n_x - q_x} \end{bmatrix}.$$

This matrix transforms the state vector into the "tracked states" vector $\mathbf{x}_q = E_x \mathbf{x}$ that contains only the states whose evolution is equal in all scenarios. In this work, $q_x = d$ will hold so that there are enough tracked states to consume all available control degrees of freedom.

With the aid of the tracking matrices, we can now define the tracking conditions (which, again, apply almost surely):

$$\begin{aligned} E_x(\mathbf{x}(\omega_1, t) - \mathbf{x}(\omega_2, t)) = 0,\ \forall t,\ \forall\ \omega_1, \omega_2 \in \Omega, \\ E_z(\mathbf{z}(\omega_1, t) - \mathbf{z}(\omega_2, t)) = 0,\ \forall t,\ \forall\ \omega_1, \omega_2 \in \Omega, \\ E_u(\mathbf{u}(\omega_1, t) - \mathbf{u}(\omega_2, t)) = 0,\ \forall t,\ \forall\ \omega_1, \omega_2 \in \Omega. \end{aligned} \tag{6}$$

The tracking conditions enforce equality in the tracked variables between realizations: note that $E_x(\mathbf{x}(\omega_1, t) - \mathbf{x}(\omega_2, t))$ is the vector of differences between the tracked states in outcome ω_1 and the tracked states in outcome ω_2. The other two conditions are analogous tracking conditions for the dependent variables and the controls.

Let us define a Bolza type functional in optimal control problems:

$$\hat{J} = \Phi(t_0, t_f, \mathbf{x}(w, t_0), \mathbf{x}(w, t_f)) + \int_{t_0}^{t_f} \mathscr{L}(\mathbf{x}(w,t), \mathbf{z}(w,t), \mathbf{u}(w,t), \xi(w), t) dt.$$

For each possible scenario or realization of the random parameters $\xi(\omega)$, we have an objetive value of $\hat{J}$. In order to build a scalar objective function, we rely on both expectations and dispersions. Without of generality, the latter can be characterized using central moments, the range, or the interquartile range (IQR), just to mention a few.

Let us then define the range R of $\hat{J}$ as

$$R(\hat{J}) = \left(\max_{\omega \in \Omega} \hat{J} - \min_{\omega \in \Omega} \hat{J} \right).$$

Let us also define the n^{th} central moment of $\hat{J}$ as:

$$\mu_n(\hat{J}) = \mathbb{E}\left[(\hat{J} - \mathbb{E}[\hat{J}])^n \right].$$

The objetive function can then be defined as:

$$\min J = \mathbb{E}[\hat{J}] + k_R \cdot R(\hat{J}) + k_{\mu_i} \cdot \mu_i(\hat{J}),\ i = 1 \dots n;$$

where k_R and k_{μ_i} $(i = 1 \dots n;)$ are generic weighting parameters.

Problem 3.1. *The robust optimal control problem with tracking (ROCT) can be defined as:*

$$minJ = \mathbb{E}[\hat{J}] + k_R \cdot R(\hat{J}) + k_{\mu_i} \cdot \mu_i(\hat{J}) \tag{7}$$

subject to (8)

$$\mathbf{x}(w, t_0) = \mathbf{x}_0; \tag{9}$$

$$\frac{d}{dt}\mathbf{x}(w,t) = f(\mathbf{x}(w,t), \mathbf{z}(w,t), \mathbf{u}(w,t), \xi(w), t); \tag{10}$$

$$h(\mathbf{x}(w,t), \mathbf{z}(w,t), \mathbf{u}(w,t), \xi(w), t) = 0; \tag{11}$$

$$g_L \leq g(\mathbf{x}(w,t), \mathbf{z}(w,t), \mathbf{u}(w,t), \xi(w), t) \leq g_U; \tag{12}$$

$$\mathbb{E}\left[\Psi(t_f, \mathbf{x}(w, t_f))\right] = 0; \tag{13}$$

$$E_z(\mathbf{z}(\omega_1, t) - \mathbf{z}(\omega_2, t)) = 0,\ \forall t,\ \forall\ \omega_1, \omega_2 \in \Omega; \tag{14}$$

$$E_u(\mathbf{u}(\omega_1, t) - \mathbf{u}(\omega_2, t)) = 0,\ \forall t,\ \forall\ \omega_1, \omega_2 \in \Omega \tag{15}$$

$$E_x(\mathbf{x}(\omega_1, t) - \mathbf{x}(\omega_2, t)) = 0,\ \forall t,\ \forall\ \omega_1, \omega_2 \in \Omega; \tag{16}$$

where in the above: $\mathbb{E}[\cdot]$ *is the expectation operator associated with the probability space* $(\Omega, \mathscr{F}, P)$*;* $\hat{J}$ *is Bolza type functional with* $\mathbb{R} \times \mathbb{R} \times \mathbb{R}^{n_x} \times \mathbb{R}^{n_x} \to \mathbb{R}$ *with a*

terminal cost or Mayer term $\Phi : \mathbb{R} \times \mathbb{R} \times \mathbb{R}^{n_x} \times \mathbb{R}^{n_x} \to \mathbb{R}$ *and running cost or Lagrange term* $\mathscr{L} : \mathbb{R}^{n_x} \times \mathbb{R}^{n_z} \times \mathbb{R}^{n_u} \times \mathbb{R}^{n_\xi} \times \mathbb{R} \to \mathbb{R}$*;* k_R *and* k_{μ_i} *(*$i = 1 \ldots n$*;) are generic weighting parameters;* f*,* h*,* g *denote the differential-algebraic equations and constraints* (3) (4) (5)*;* E_x*,* E_y*,* E_z *are the tracking conditions* (6)*; and function* $\Psi : \mathbb{R} \times \mathbb{R} \times \mathbb{R}^{n_x} \times \mathbb{R}^{n_x} \to \mathbb{R}^{n_x}$ *denotes the final conditions.*

3.2. Objective function

We want to find routes that minimize a weighted sum of average flight time and average fuel consumption (weighted with the Cost Index CI factor), flight time dispersion (weighted with the "dispersion penalty" parameter DP) and exposure to convective risk (weighted with the "convection penalty" parameter CP).

We model convective conditions (recall that they are necessary though not sufficient conditions) with the function $c(\phi, \lambda, t)$, where ϕ denotes latitude and λ longitude. Given the latest EPS forecast available at planning time t_p, this function represents the fraction of the EPS members forecasting that two indicators of convective conditions (TT and CP) will exceed their thresholds at point (ϕ, λ) and at time t. For convenience, we assume that the planning time t_p is unambiguous and denotes the function $c(\phi, \lambda, t)$.

Assume now that an aircraft has a trajectory described by the time domain $\mathscr{T} = [t_0, t_f]$, the groundspeed profile $v_g(t)$, and a lateral profile described by $(\phi(t), \lambda(t))$. Let $c(\phi, \lambda, t)$ be the smoothed and interpolated probability of convection and let the exposure to convection (EC) be:

$$EC = \int_{t_0}^{t_f} c(\phi(t), \lambda(t), t) \cdot v_g(t) \cdot dt. \tag{17}$$

Assume now that the flight planner has time-fuel preferences described by a Cost Index (CI) and average cost - uncertainty cost preferences described by a

Dispersion Penalty (DP) parameter, i.e., the cost functional is given by

$$J = \underbrace{-\mathbb{E}[m(t_f)] + CI \cdot \mathbb{E}[t_f]}_{\text{Cost-Index based operational cost}} + \underbrace{CP \cdot \mathbb{E}[EC]}_{\text{Cost of exposure to convection}} + \underbrace{DP \cdot R[t_f]}_{\text{Cost of arrival time dispersion}} \tag{18}$$

where $R[t_f]$ represents the uncertainty in the arrival time as given by the range of possible final times, and $m(t_f)$ denotes the mass of the aircraft at the final time. Notice thus that we are not considering central moments, though the formulation can be also applied by considering them.

With this cost functional, the parameters CI, DP, and CP regulate the solution flight plan depending on the preferences of the flight planner. High values of DP will produce more predictable trajectories (not considering potential convection-related reroutes) by avoiding regions where the wind is more unpredictable. High values of CP will produce trajectories that are less likely to be rerouted by avoiding regions where there is a high likelihood of convection. Low values of the parameters will produce flight plans that are more efficient on average, but less predictable. In turn, the CI parameter weights the preferences in terms of flight time and fuel burn. A higher CI[6]. would result in a preference for flying faster at the toll of consuming more fuel, which might be convenient when connecting flights. While the latter (CI) is commonly used by airlines on a daily basis, neither the cost of being predictable nor the cost of reducing exposition to convective areas is being considered in today's practices.

[6] It should be noted that we will use the International System Units, i.e., kg/sec. for the CI. Please note that this would result in values that are far form those used in commercial aircraft, which typically use kg/min

3.3. Aircraft dynamics

We restrict ourselves to a constant altitude flight.[7] As this is a routing problem, turning dynamics become relatively unimportant. BADA 4[8] will be used as the aircraft performance model, which among other features, incorporates a non-parabolic drag polar that takes compressibility effects into consideration. This is needed to obtain meaningful results since flight optimization tools/algorithms based on BADA 3 (which incorporate a parabolic drag polar) are known to underestimate drag at high speed (near the transonic regime), resulting in unrealistic speed profiles. See for instance [**?**]

Thus, the differential equations governing the 3-DoF motion of the aircraft are:

$$\dot{\mathbf{x}} = \frac{d}{dt}\begin{bmatrix}\phi\\ \lambda\\ v\\ m\end{bmatrix} = \begin{bmatrix}\dfrac{v\cos(\chi)+w_x}{(R_N+h)}\\ \dfrac{v\sin(\chi)+w_y}{(R_M+h)\cos\phi}\\ \dfrac{(T-D)}{m}\\ -f_c(C_T)\end{bmatrix}, \tag{19}$$

where the drag (D) is computed according to the assumption that the lift force is equal to the weight. In Equation (19), v denotes the true airspeed, m the mass, χ the heading angle, w_x and w_y the zonal and meridional wind components, respectively, R_N and R_M the Earth's (modelled as an ellipsoid) radius of curvature in the prime vertical and the meridian, respectively, ϕ the bank angle, T the thrust force, and f_c is a fuel consumption function that depends on a coefficient of Thrust (C_T).

We will also consider the following constraints that are related to the airspeed and the thrust limits:

[7] Note, however, that the methodology can be extended to full 4D problems since direct methods are flexible enough that they can handle more complex problems; we choose our assumptions, which are comparable to most of the published routing algorithms, for simplicity.

[8] https://simulations.eurocontrol.int/solutions/bada-aircraft-performance-model/

$$
\begin{aligned}
v_{CAS,stall} \leq v_{CAS}(v) \leq v_{CAS,max}, \\
M(v) \leq M_{max}, \\
T_{idle}(v) \leq T \leq T_{max},
\end{aligned}
\tag{20}
$$

where v_{CAS} denotes the calibrated airspeed and M the Mach number.

3.4. Problem statement

We do the following manipulations to reformulate the problem (details can be found in [**?**]):

- Let us reformulate this dynamical system as a differential-algebraic system (DAE) with the addition of the ground speed v_G as an algebraic variable and the course ψ as a control variable, linked to the remaining variables by two new equality constraints. This is advantageous for computational purposes and for clarity of exposition.

- In the robust optimal control framework, the independent variable (time) is unique in all scenarios (it varies in the same range). Therefore, the direct application of the state-tracking formulation would demand the position of the aircraft to be in a fixed schedule with respect to time in all scenarios, and thus the groundspeed would be fixed. This implies that, under this concept, the variability in wind speed would be fully compensated by airspeed modifications, with associated variations in fuel burn. Thus, we will employ distance flown along the route (s) as the independent variable, because its initial and final values are the same in all scenarios that follow a unique route. As a consequence, the time t becomes a state variable and the new dynamical function can be obtained by dividing the time derivatives by $ds/dt = v_G$. We also define $a := dv/ds$ for practical purposes, to combine the derivative of v and its tracking condition in a single set of constraints. Its physical interpretation is the slope of the airspeed profile.

- The robust optimal control framework requires the formulation of the trajectory ensemble. An ensemble forecast contains a set of ensemble members,

each one defining a different wind forecast (and, therefore, different functions w_x and w_y). If the ensemble contains N members, we define N scenarios, each one having a weight of $w_k = 1/N$ and the wind field that corresponds to the respective member.

Taking advantage of these manipulations, we can define the dynamical system associated with the trajectory ensemble with the dynamical function:

$$\frac{d\mathbf{x}_E}{ds} = \frac{d}{ds}\begin{bmatrix} \phi \\ \lambda \\ v \\ t_1 \\ \vdots \\ t_N \\ m_1 \\ \vdots \\ m_N \end{bmatrix} = \begin{bmatrix} \cos(\psi)/(R_N + h) \\ \sin(\psi)/(R_N + h)\cos\phi \\ a \\ 1/v_{\mathrm{G},1} \\ \vdots \\ 1/v_{\mathrm{G},N} \\ -f_c T_1/v_{\mathrm{G},1} \\ \vdots \\ -f_c T_N/v_{\mathrm{G},N} \end{bmatrix}, \tag{21}$$

with the control vector:

$$\mathbf{u}_E = \begin{bmatrix} a & \psi & T_1 & \dots & T_N & \chi_1 & \dots & \chi_N \end{bmatrix}^T,$$

the equality constraints:

$$\begin{bmatrix} v_{\mathrm{G},1}\cos(\psi) \\ \vdots \\ v_{\mathrm{G},N}\cos(\psi) \\ v_{\mathrm{G},1}\sin(\psi) \\ \vdots \\ v_{\mathrm{G},N}\sin(\psi) \\ a \cdot v_{\mathrm{G},1} \\ \vdots \\ a \cdot v_{\mathrm{G},N} \end{bmatrix} = \begin{bmatrix} v\cos(\chi_i) + w_{x,1} \\ \vdots \\ v\cos(\chi_i) + w_{x,N} \\ v\sin(\chi_i) + w_{y,1} \\ \vdots \\ v\sin(\chi_i) + w_{y,N} \\ (T_1 - D_1)/m_1 \\ \vdots \\ (T_N - D_N)/m_N \end{bmatrix}, \tag{22}$$

and the inequality constraints:

$$\begin{gathered} v_{CAS,stall} \leq v_{CAS}(v) \leq v_{CAS,max}, \\ M(v) \leq M_{max}, \\ \left.\begin{array}{l} T_{idle}(v) \leq T_k \leq T_{max} \\ 0 \leq v_{G,k} \end{array}\right\} \forall k \in \{1, \dots \ N\} \end{gathered} \quad . \tag{23}$$

Note that $\mathbf{x}_E$ and $\mathbf{u}_E$ denote extended state and control vectors termed state ensemble and control ensemble, respectively.

4. Case Study

4.1. Description

We consider a BADA4 A330 Aircraft model flying from the vertical of New York (-73.8 deg, 40.6 deg) to the vertical of Argel (3.2 deg, 36.7 deg) at constant barometric altitude 200hPa. Initial mass and initial Mach have been set to 200 tons and M=0.82, respectively. We use a forecast for a pressure of 200 hPa 9 hours in advance for the 19th of December, 2016 from the ECMWF ensemble with 51 members. The relevant variables for our purposes are the values at isobaric levels of the temperature T, the geopotential height H, the total totals (TT), the Convective Precipitation (CPre), and the zonal and meridional components of the wind $\mathbf{v}_w$. These fields will be spatially interpolated through cubic b-splines to produce a continuous and smooth field that can be employed in optimal control. We rely on a constant weather picture for ease of exposition and analysis. We rely on the CasADi library [**?**] as NLP interface [**?**] and IPOPT [**?**] as NLP solver running with the MA27 sparse symmetric linear solver from the HSL Mathematical Software Library and initial barrier parameter $\mu = 10^{-3.8}$. The computations are performed in a workstation equipped with an Intel(R) Core(TM) i5-3570K CPU running at 3.40GHz and with 16Gb RAM. We employ a trapezoidal transcription scheme with piecewise-constant controls as direct collocation method. In any case, other discretization methods are suitable for this work.

The NLP model used to solve this problem had 12002 variables, 11924 equality constraints, and 9852 inequality constraints. Focusing on, e.g., the case with parameters DP0.2 CP=0.1 CI=0 (needless to say, computational performance is similar for all the cases), IPOPT solver took 50 iterations to find a solution with a computation time in IPOPT function evaluations (time spent in the MA27 linear solver and solving the Karush-Kuhn-Tucker) of 1674.7 sec., and a computation time in NLP function evaluations (time spent in objective, gradient, Jacobian, and Hessian functions) of 110.4 secs.

4.2. Results and discussion

We first show results sweeping values for each of the parameters in the objective function, namely CP, DP, and CI. Figure 2 shows the geographical paths: while they do not change significantly when modifying CI (setting $CP = 0$ and $DP = 0$), it can be seen that routes computed with higher DP (setting $CP = 0$ and $CI = 0$) tend to avoid the high uncertainty zone in the North Atlantic to increase predictability, at the cost of taking a more indirect route that is expected to be longer. It can be also observed that routes computed with higher CP (setting $DP = 0$ and $CI = 0$) tend to reduce the exposure to convective risk zones, again at the cost of taking a more indirect route.

Figure 3-4 shows the evolution of relevant state/control variables in the problem, namely true airspeed (TAS), coefficient of thrust (CT), coefficient of lift (CL), and mass (m). The effects of each of the penalty parameters can be readily seen therein. It can be observed that the main influence in the airspeed profile is the variation in the CI, as expected, the higher it is is, the higher the airspeed values along the whole trajectory. The CP parameter does not have a big influence on the shape of the airspeed profile, which changes as the lateral path shifts to a different location. Finally, in those cases with high DP the airspeed changes locally depending on the uncertainty of the winds at each

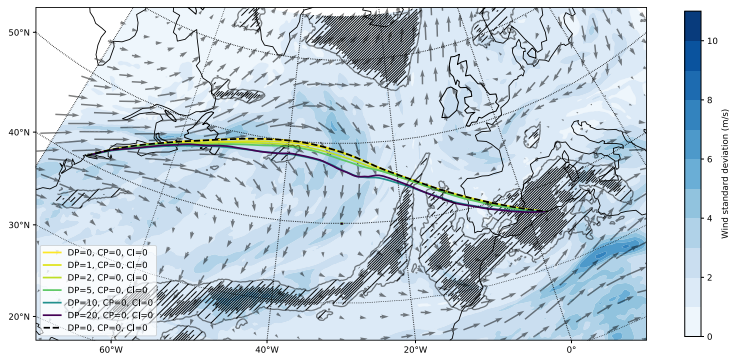

(a) Optimal paths with different DP values (CP = 0 and CI = 0).

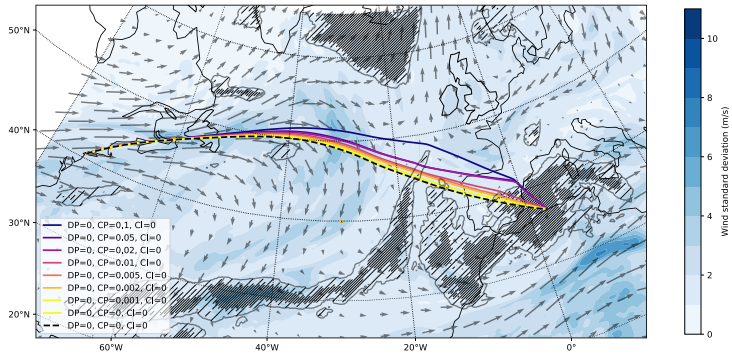

(b) Optimal paths with different CP values (DP = 0 and CI = 0).

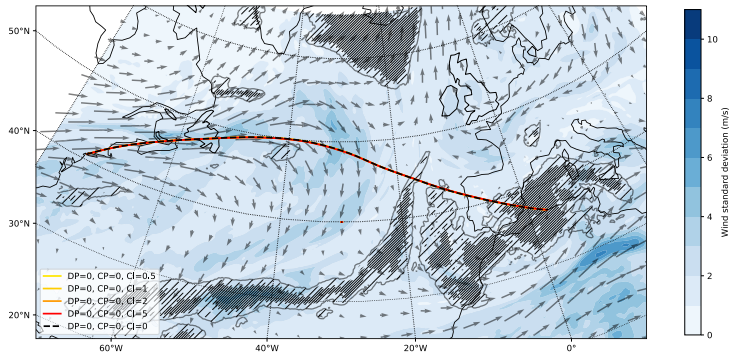

(c) Optimal paths with different CI values (DP=0 and CP=0).

Figure 2: Optimal trajectories for different CP/DP/CI values. Color contour scale indicates wind uncertainty characterized as $\sqrt{\sigma_u^2 + \sigma_v^2}$, with σ_u being the standard deviation of the u component of wind across different members and σ_v analogous for the v-component. Dashed regions indicate regions of convective exposure.

point in the trajectory, with higher airspeeds when the aircraft crosses higher uncertainty zones. This influence is moderated by higher CI settings.

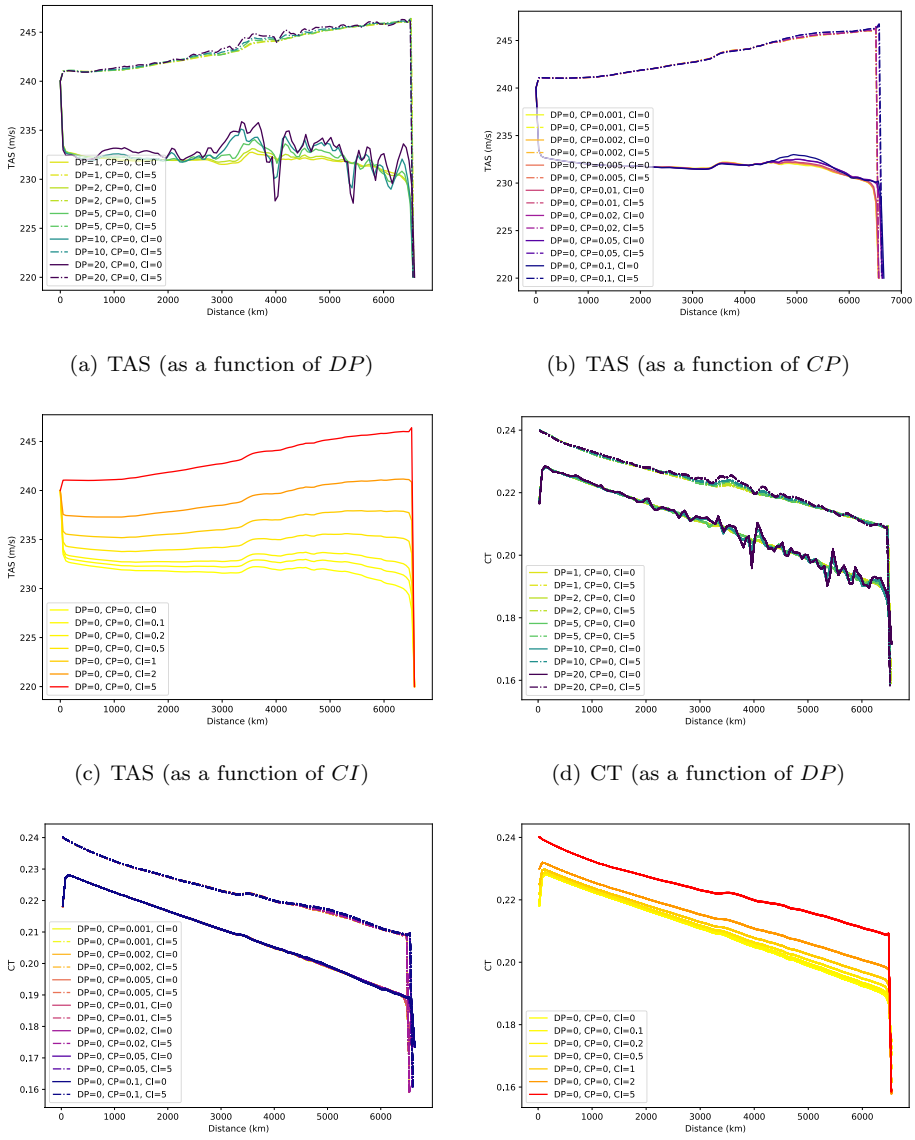

(a) TAS (as a function of DP)

(b) TAS (as a function of CP)

(c) TAS (as a function of CI)

(d) CT (as a function of DP)

(e) CT (as a function of CP).

(f) CT (as a function of CI)

Figure 3: Evolution of TAS, CT, CL, and mass over time

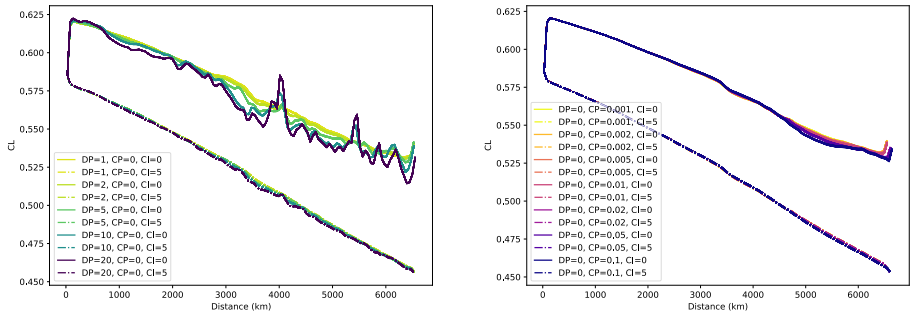

(a) CL (as a function of DP)

(b) CL (as a function of CP)

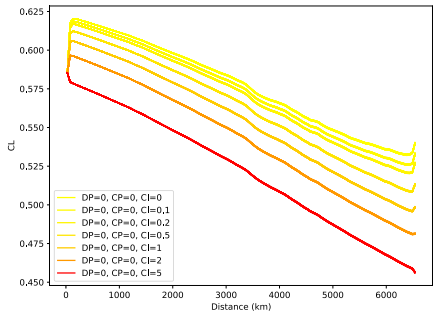

(c) CL (as a function of CI)

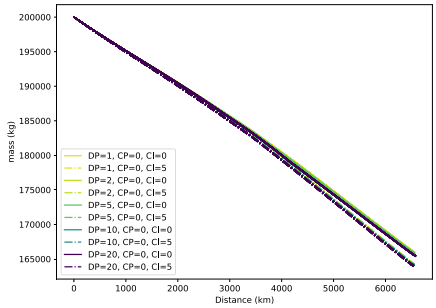

(d) m (as a function of DP)

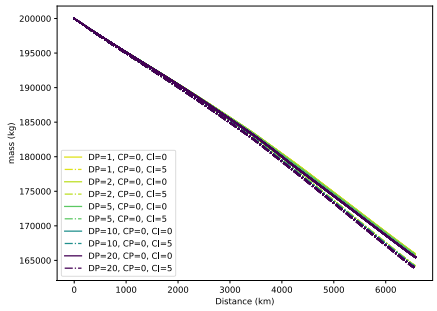

(e) m (as a function of CP)

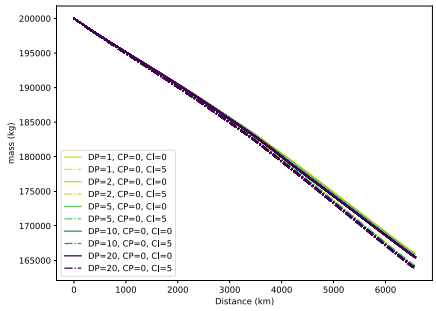

(f) m (as a function of CI)

Figure 4: Evolution of TAS, CT, CL, and mass over time

4.2.1. Featured trajectories

In order to discuss and better analyse the different phenomena, we have featured 8 trajectories with different parameter values that illustrate the effects

of each of them in the solution. Parameter values can be consulted in Table 2.

	DP	CP	CI
Trj. #1	0	0	0
Trj. #2	0	0	5
Trj. #3	0	0.1	0
Trj. #4	0	0.1	5
Trj. #5	10	0	0
Trj. #6	10	0	5
Trj. #7	10	0.1	0
Trj. #8	10	0.1	5

Table 2: Featured trajectories: parameter values.

Figure 5 illustrates the optimal paths of these featured trajectories. The clearest interaction takes place when CI increases since it "pulls back" the trajectories with higher CP and DP values towards the optimal trajectory on average; this can be explained by the fact that the dispersion and convection terms lose relative weight as CI increases. The other interaction that can be observed is that, when DP is increased at high CP, the optimal trajectory shifts even more towards the North instead of being pulled South towards the "high DP" solution, which illustrates the nonlinear effects caused by the non-convexity of the uncertainty and convection fields.

We show the evolution of the time dispersion along the trajectory in Figure 6. In this chart, we plot the flyby times at each point in the trajectory for each of the 50 ensemble members. It can be observed that higher DP settings lead to tighter uncertainty profiles, just as expected; however, this trend is moderated

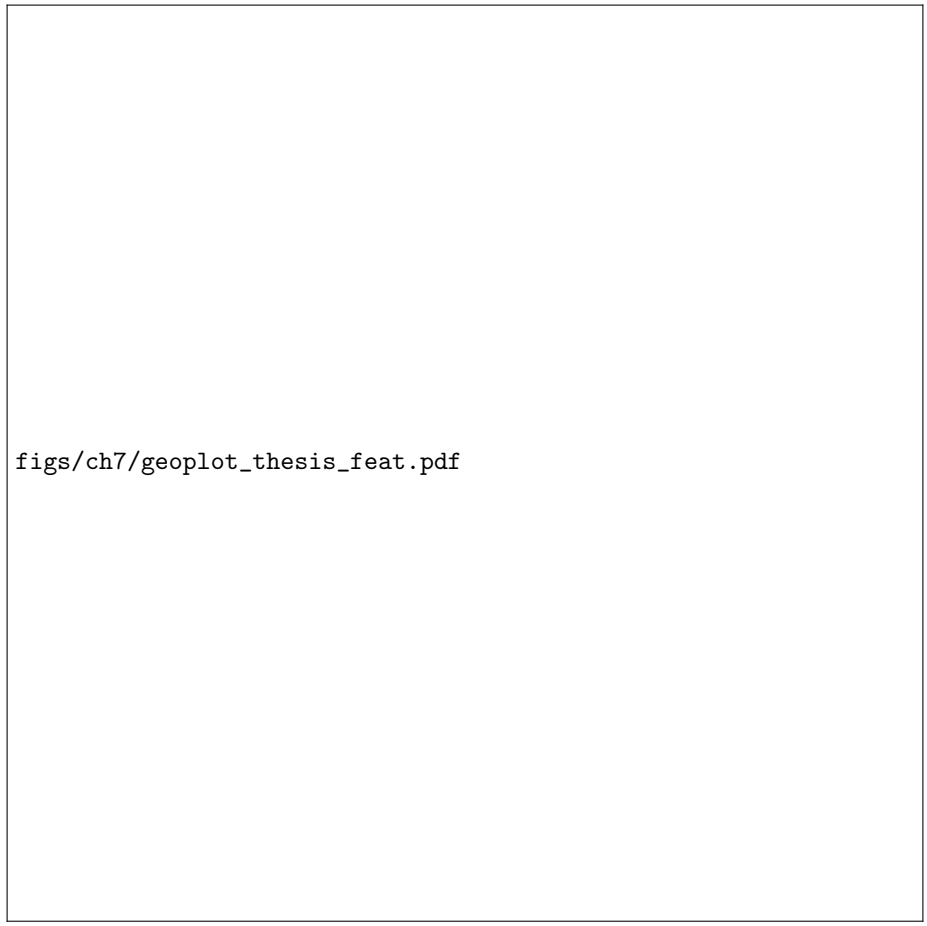

Figure 5: Optimal paths of featured trajectories. Color contour scale indicates wind uncertainty characterized as $\sqrt{\sigma_u^2 + \sigma_v^2}$, with σ_u being the standard deviation of the u component of wind across different members and σ_v analogous for the v-component. Dashed regions indicate regions of convective exposure.

by the increase in the other parameters (particularly the CI), since the relative importance of reducing dispersion due to wind uncertainty decreases.

Figure 7 illustrates the probability of convection $c(\phi, \lambda, t)$ along the route (compare with Figure 5 to see how the segments of a high probability of convective conditions correspond to the crossing of the highlighted regions). Again, it is clear that a higher CP parameter emphasizes avoidance of areas of likely

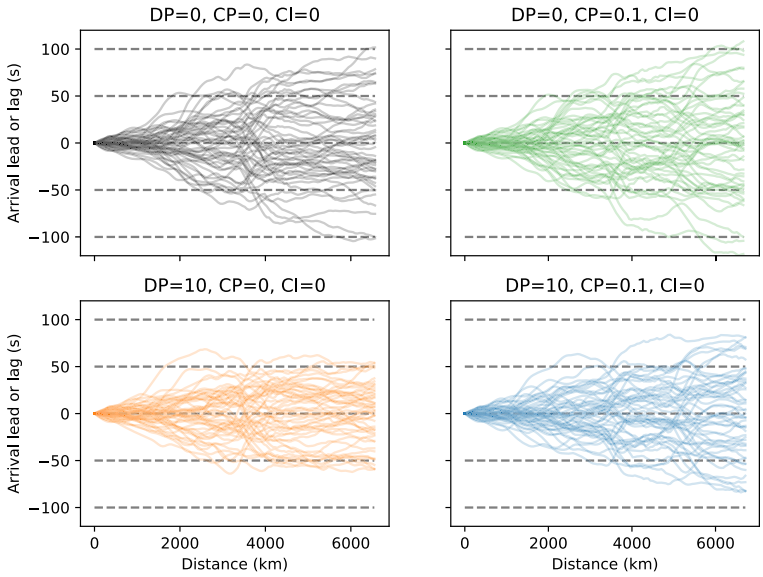

(a) CI=0

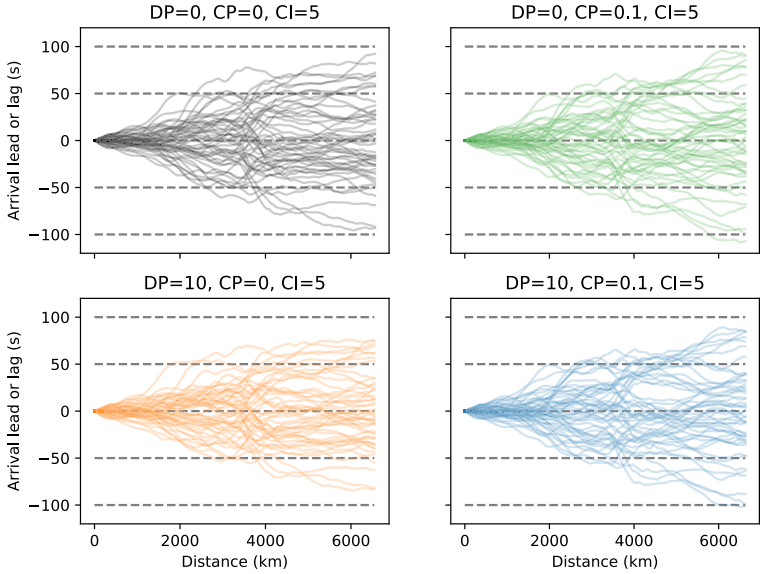

(b) CI=5

Figure 6: Evolution of time dispersions for the different ensemble members.

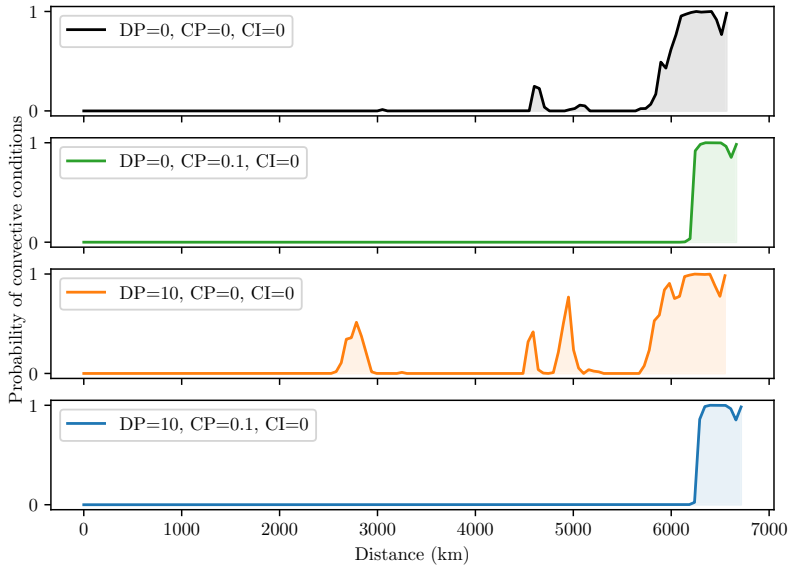

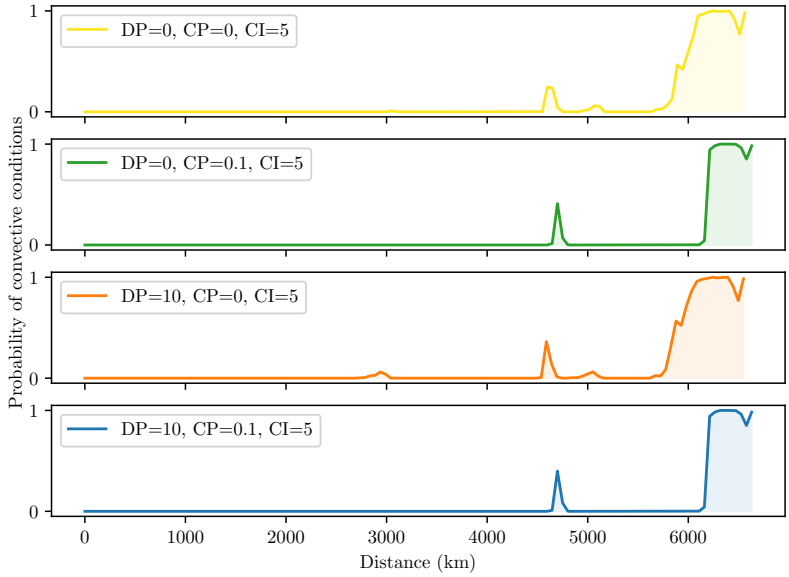

(b) CI=5

Figure 7: Evolution of the convective exposure.

convective conditions; the trajectories generated with CP=0.1 only encounter (unavoidable) risk of convection at the end of the trajectory, near the final fix.

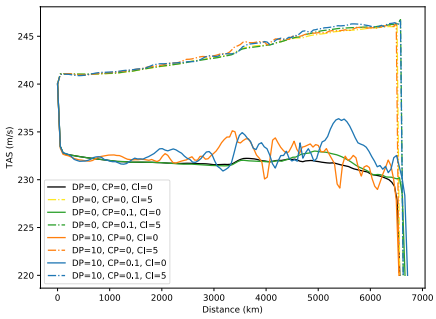

(a) Optimal TAS profiles.

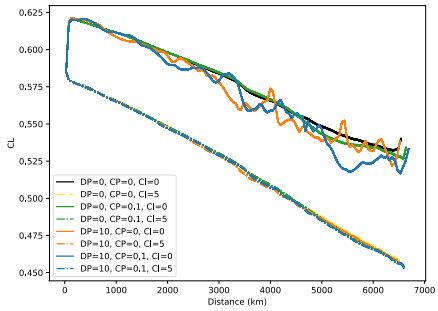

(b) Optimal CL profiles.

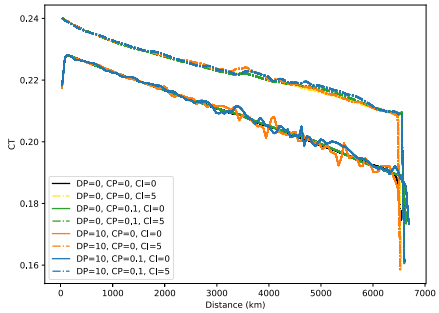

(c) Optimal CT profiles.

Figure 8: Optimal profiles for the features trajectories.

Figure 8 shows the respective airspeed profiles. Together with the airspeed profiles, coefficient of lift (CL), coefficient of thrust (CT) and mass of the vehicle are presented. Clearly, at high CI values, the airspeed profiles also become high and very similar. The airspeed profiles for the low CI trajectories show more variability between them, which should be expected as they fly different lateral paths and thus face different winds. Finally, the "speed-up on higher wind uncertainty" effect is also clearly present for the trajectories with high DP but low CI. Again, a higher CI setting has a regularizing effect, leading to smoother airspeed profiles as the relative influence of the wind and its uncertainty is reduced. It can be also observed how high CI values result in high CT values and high CL values, in other words, in other to fly faster we need more thrust and less CL is needed to balance lift with weight. Also, we can observe how fuel

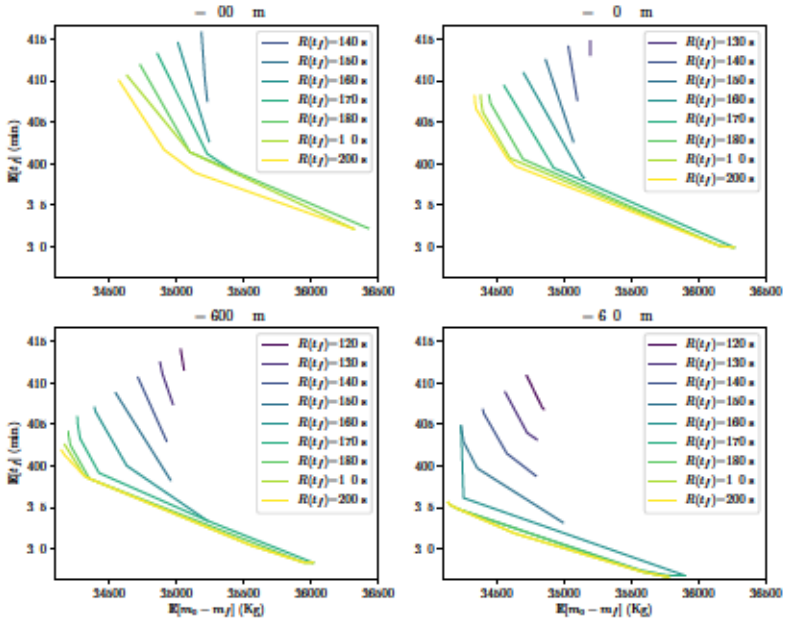

Figure 9: Trade-offs (Pareto fronts) for fixed exposure to convective risk and flight time dispersions.

is being burnt and, thus, the mass of the aircraft decreases.

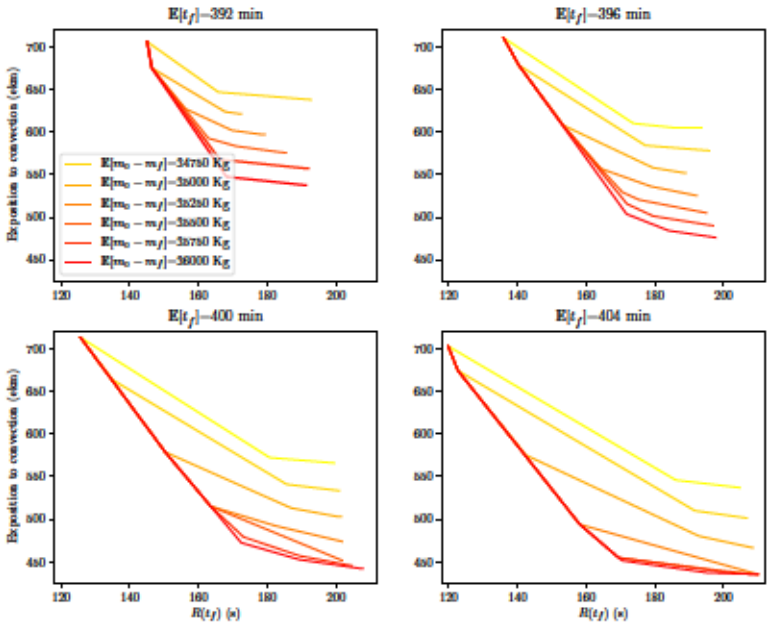

Figure 10: Trade-offs (Pareto fronts) for fixed average flight times and average fuel consumptions.

Finally, we illustrate the trade-offs that are available to the flight planner.

In Figure 9, we illustrate the trajectory options in terms of the average performance, which can be obtained for selected amounts of uncertainty (both from time spread and convection). In first place, it can be observed that the cost of reducing uncertainty due to wind has a nonlinear shape, with the level curves being relatively closer between 200 s and 180 s of arrival time range than between 180 s and 130 s. in other words, using airspeed variations allows the algorithm to cheaply improve predictability up to a point where it saturates or becomes inefficient; afterwards, the more expensive lateral path modifications need to be employed and the cost of reducing the arrival time window ($R[t_f]$) by 10 seconds is between 100 to 200 kg ($\mathbb{E}[m_0 - m_f]$) on average or 3 to 6 minutes (($\mathbb{E}[t_f]$)). Reducing exposure to convection appears to have a more

homogeneous penalty in terms of cost, with the cost of encountering 50 ekm[9] less of potential convective conditions being on the order of 5 to 10 minutes or 100 to 200 kilograms of average fuel consumption.

In Figure 10, we can observe the uncertainty that a trajectory will face for a given average performance (in terms of average flight time or average fuel consumption). We can again observe the mentioned nonlinearity: at higher dispersion in the arrival time, the cost to reduce it (now in terms of exposition to convection at fixed $\mathbb{E}[t_f]$ and $\mathbb{E}[m_0 - m_f]$) is smaller. This can be readily seen looking at the the level curves, which are flatter at the right of the kink point. However, they become steeper at the left of this point. The mentioned trade-offs between exposition to convection and average performance can also be observed more clearly in this graph: at around 180 seconds of arrival window size, 250 kg of average fuel burn can reduce exposition to convection by 15 to 20 ekm in faster flights and by 30 to 40 ekm in later arrivals. In other words, at high CI settings (faster flights), where the flight time is more relatively important, predictability improvements are more expensive in terms of average fuel burn than they are at slower flights, as the algorithm has more "room" to tune the flight plan.

5. Conclusions and future work

A robust optimal control methodology has been used for computing efficient and predictable routes based on Ensemble Prediction Systems, including an approach to calculate the risk of convection. This risk, a necessary though not sufficient condition for the formation of storms, has been included in the objective functional of the robust optimal control problem. This cost combines other objectives, such as flight time predictability or a cost-index based operational performance. We have demonstrated its utility in studying trade-offs between operational performance (measured in terms of average flight times and fuel

[9] ekm denotes equivalent kilometers, i.e., the kilometers flown under hypothetical probability of convection equal to one

consumption, and weighted by a cost index), predictability (measured in terms of dispersion in the final time) and exposure to convection. Pareto-optimal solutions have been presented and discussed. We can conclude that uncertainty (in this case due to wind) can not only be quantified but also reduced by proposing alternative trajectories. Also, convective areas can be avoided at the cost of predictability and operational efficiency. The latter can be regulated by the selection of the cost-index value. All in all, a portfolio of solutions can be made available to flight dispatchers to select its prefer planning strategy by tuning the three parameters (DP, CP, and CI) that regulate the different objectives of the problem (dispersion, convective exposure, and operational efficiency).

Future directions of research are twofold: on one hand, the extension of this work to three-dimensional flights, which would permit the analysis of uncertainties associated to the top-of-climb and top-of-descent and the modelling of airport-to-airport problems. An important challenge would be related to growth in the number of states and controls, which in the robust approach presented herein grow with the number of members in the ensemble. Also, modelling the ceiling of the convection area would be of interest for vertical avoidance. To circumvent these challenges, a second direction of research interest would be to explore heuristic approaches, which would allow the consideration of realistic flight planning problems, including structured airspaces and decision-making.

6. Acknowledgments

This work has been partially supported by project TBO-MET project (https://tbomet-h2020.com/), which has received funding from the SESAR JU under grant agreement No 699294 under European Union's Horizon 2020 research and innovation programme.

References